Autologous tumor-derived microvesicles influence gene expression profiles and enhance protumorigenic chemotactic potential, signal transduction and cellular respiration in gastric cancer cells

RAFAL SZATANEK[1], KAZIMIERZ WEGLARCZYK[1], MALGORZATA STEC[1], JAROSLAW BARAN[1], MAGDALENA PARLINSKA-WOJTAN[2], MACIEJ SIEDLAR[1] and MONIKA BAJ-KRZYWORZEKA[1]

[1]Department of Clinical Immunology, Jagiellonian University Medical College, 30-663 Krakow; [2]Institute of Nuclear Physics Polish Academy of Sciences, 31-342 Krakow, Poland

Received April 18, 2019; Accepted October 18, 2019

DOI: 10.3892/ijo.2019.4923

Abstract. Tumor-derived microvesicles (TMVs) interact with a variety of different cell types within the immune system, including lymphocytes, monocytes, dendritic cells and tumor cells that they have originated from. In the present study, the effects of autologous-TMVs (auto-TMVs) on gene expression, chemotaxis, intercellular signaling and cellular metabolism were examined in cells of the gastric cancer (GC) cell line 1415 (GC1415). The effects of auto-TMVs on mRNA gene expression in GC1415 cells were assessed using pathway-focused PCR arrays. A chemotaxis assay was performed using the HoloMonitor M4 System. Signaling pathways were evaluated using western blot analysis, and cellular respiration was measured using the Seahorse XF Cell Mito Stress Test. Exposure of the GC1415 cells to auto-TMVs led to the overexpression (75 genes) and underexpression (96 genes) of genes that are associated with signal transduction, metabolism, chemotaxis, angiogenesis and metastasis. The auto-TMVs were indicated to induce chemotaxis and activate the PI3K/AKT signaling pathway in GC1415 cells. However, the MAPK/ERK signaling pathway was not indicated to be activated. Furthermore, studies on cellular respiration in GC1415 cells exposed to auto-TMVs demonstrated a metabolic shift to glycolysis. The results of the current study thus indicate that auto-TMVs may exert an effect on tumor cell function.

Correspondence to: Dr Rafal Szatanek, Department of Clinical Immunology, Jagiellonian University Medical College, ul. Wielicka 265, 30-663 Krakow, Poland
E-mail: rafal.szatanek@uj.edu.pl

Abbreviations: TMVs, tumor-derived microvesicles; EVs, extracellular vesicles; GC, gastric cancer; NTA, nanoparticle tracking analysis

Key words: tumor-derived microvesicles, gastric cancer, extracellular vesicles

Introduction

New gastric cancer (GC) cases have declined by 40% worldwide over the past 50 years (1-3). However, GC continues to be a significant public health concern (1-3). GC is the third most common type of cancer and the second leading cause of cancer-associated mortality worldwide (4,5). It has been estimated that globally, GC accounts for 989,600 new cases and 738,000 deaths annually, rendering its case-fatality ratio higher compared with other common malignancies, including colon, breast and prostate cancer (3).

Extracellular vesicles (EVs) are small membrane sacs that are released by a variety of cell types under normal or pathological conditions (6). Previously known as 'cellular dust', EVs are now recognized as important mediators during cell-to-cell communication (6). It has been demonstrated that EVs transport bioactive cargo between cells in the form of transmembrane receptors, mRNAs, microRNAs (miRNAs or miRs) and signaling molecules, which are able to modify the extracellular microenvironment (6-10). For example, cancer EVs carrying transforming growth factor β (TGF-β) have been indicated to induce fibroblast differentiation into cancer associated fibroblasts with increased levels of α-smooth muscle actin (11). A previous study also demonstrated that exosomes containing extracellular matrix metalloprotease (MMP) inducer, which is released by lung carcinoma cells, enhanced MMPs in fibroblasts and led to tumor progression and metastasis (12). Wieckowski *et al* (13) demonstrated that EVs isolated from head and neck squamous cell carcinoma cells expressed melanoma-associated antigen 3/6 and Fas ligand, and were able to induce apoptosis in $CD8^+$ T lymphocytes. The aforementioned studies indicated that cancer cells may release EVs to escape immunological surveillance by exerting a direct effect on normal cells. There is increasing evidence that cancer cells may also communicate via autologous EV release to impair an effective anti-tumor response from the immune system. Gamperl *et al* (14) revealed that microparticles containing tissue factor that were isolated from pancreatic adenocarcinoma cells were able to induce cell migration in tumor cells by activating the protease activated receptor 2 (PAR2) signaling pathway. An additional study demonstrated

that EVs derived from pancreatic cancer cells led to the down-regulation of Hes-1 transcription factor, an intracellular target of the Notch-1 signaling pathway, which was indicated to induce the apoptosis of these cells (15). Al-Nedawi *et al* (16) reported that glioblastoma (GMB)-derived EVs containing epithelial growth factor receptor variant III (EGFRvIII) were transferred from EGFRvIII-positive GMB cells to EGFRvIII-negative GMB cells, which led to the activation of the mitogen-activated protein kinase (MAPK) and Akt signaling pathways, and resulted in the expression of vascular endothelial growth factor (VEGF).

The subject of the current study was the human GC cell line, GC1415 (patent pending), of Caucasian origin that was previously established and characterized in our laboratory (17). The aim of the present study was to investigate whether the autologous tumor-derived microvesicles (auto-TMVs) released by GC1415 cells are capable of altering the following: i) Gene expression; ii) chemotactic potential; iii) signal transduction; and iv) cellular respiration in GC1415 cells that are exposed to them.

Materials and methods

Isolation of TMVs. Cells of the previously characterized GC1415 cell line (17) were cultured using bi-weekly passages in DMEM (GE Healthcare) supplemented with 5% FBS (Biowest), which was centrifuged at 50,000 x g for 1 h at room temperature to remove bovine EVs. The cells were regularly tested for *Mycoplasma sp*. contamination using a PCR-ELISA kit (Roche Diagnostics GmbH) and for endotoxin contamination using a Limulus test (Charles River Laboratories, Inc.), according to the manufacturers' protocols. Supernatants from cell cultures were collected at ~90% confluency and centrifuged using a modified protocol that was previously described (18). Briefly, the collected supernatants were spun at 3,000 x g for 10 min at room temperature to remove cellular debris and transferred to a new Eppendorf-type test tube and spun again for 30 min at 13,000 x g at room temperature. Supernatants were subsequently transferred to new Eppendorf-type test tube and centrifuged for 2 h at 100,000 x g at 4˚C. Supernatants were then discarded and the remaining pellets were re-suspended in 100 μl filtered (0.22 μm) PBS. The auto-TMV protein concentration was obtained according to the Bradford method's protocol using Quick Start Bradford Dye reagent (Bio-Rad Laboratories, Inc.). Isolated auto-TMVs were tested for endotoxin contamination using a Limus test and stored at -20˚C until further use. Based on our previous studies, the quantity of auto-TMVs used in the subsequent experiments was determined to be 3 μg (18,19).

Nanoparticle tracking analysis (NTA). Average size, modal size and size distribution of auto-TMVs were obtained using the NANOSIGHT LM10-HS488FT14 Nanoparticle Characterization system (Malvern Instruments, Ltd.) as previously described (18). A total of 1 μl auto-TMV suspension was then diluted to 1:1,000 in filtered (0.22 μm) PBS to obtain the total sample volume of 1 ml. Subsequently, ~700 μl of the sample was loaded manually into the measuring chamber using a 1-ml insulin-type syringe (Terumo Corp.) and the syringe was mounted onto the pump to deliver the sample at a constant flow rate of 80 units. Subsequently, three 1-min videos were recorded using the sCMOS camera for each sample and analyzed using NanoSight NTA 3.1 analytical software (Malvern Instruments, Ltd.).

Scanning electron microscopy (SEM). For morphological and size analyses, auto-TMVs were fixed using 2.5% glutaraldehyde at room temperature for 10 min and particles were washed twice in PBS using an ultracentrifugation step for 30 min at 100,000 x g and 4˚C. The auto-TMV pellet was then re-suspended in 100 μl PBS, and a 20-μl suspension was applied to the double-sided adhesive conductive carbon tape (Agar Scientific, Ltd.) and allowed to air-dry for ~1 h at room temperature. The air-dried auto-TMVs were then subjected to dehydration using gentle, stepwise washing with ethanol at 50, 70, 90 and 100%. Imaging was performed using a Tescan Vega 3 scanning electron microscope (magnification, 80.1 kx) equipped with a tungsten cathode (TESCAN), which was set at the acceleration voltage of 10 kV, and a secondary electron detector.

RT-qPCR arrays. For mRNA gene expression, the GC1415 cells ($1x10^6$) were suspended in 500 μl of the DMEM (GE Healthcare) cell medium supplemented with 5% FBS (Biowest) and exposed to auto-TMVs (3 μg) for 2 h (37˚C; 5% CO_2). The same number of GC1415 cells cultured under the same culturing conditions but without the exposure to auto-TMVs was used a control. Total RNA isolation and first-strand cDNA synthesis were subsequently performed as previously described (20). The generated cDNA was used for the analyses of mRNA gene expression (in duplicate) using the pathway-focused (angiogenesis, tumor metastasis, oncogene and tumor suppressor genes) RT^2 Profiler PCR Arrays (Qiagen GmbH) according to the manufacturer's protocol. A total of 25 μl prepared PCR component mix, which included 5 μl cDNA, was added to each well of a 96-well PCR array plate and capped with cap strips. A PCR reaction was then performed (initial denaturation for 10 min at 95˚C, then 15 sec at 95˚C and 1 min at 60˚C for 40 cycles) using the 7300 Real Time PCR system (Applied Biosystems; Thermo Fisher Scientific, Inc.). Following each PCR run, a melting curve analysis was performed using 7300 System SDS software version 1.2.3 (Applied Biosystems; Thermo Fisher Scientific, Inc.) to verify the amplified PCR product. The obtained PCR array data were analyzed using the on-line Data Analysis Center (Qiagen GmbH).

Chemotaxis assay. The chemotaxis assay was performed using the µ-slide chemotaxis set (ibidi GMbH) according to the manufacturer's protocol. At 1 day prior to the experiment, all components of the µ-slide chemotaxis set, including the slide, caps, plugs and cell medium (DMEM + 5% FBS) were placed in a CO_2 incubator (37˚C; 5% CO_2) overnight for gas equilibration. Additionally, the microscope component of the HoloMonitor M4 system (Phase Holographic Imaging AB) was switched on and left overnight inside the CO_2 incubator to achieve parameter stability. The following day, a total of 6 μl GC1415 cell suspension (~$3x10^6$ cells/ml) was applied to the µ-slide seeding channel via its filling port. The µ-slide was then placed into a Petri dish with a sterile wet tissue surrounding

the slide and was left in the CO_2 incubator for 3 h until cell seeding was achieved. Following cell seeding, a total of 65 μl cell medium was applied to each reservoir located on the sides of the µ-slide seeding channel, according to the manufacturer's protocol. A total of 30 μl cell medium containing auto-TMVs (3 μg) was introduced into one of the reservoirs to achieve a uniform auto-TMVs gradient. All filling ports were closed with plugs apart from those of the cell seeding channel, which were covered with caps. The µ-slide was then mounted onto the microscope stage inside the CO_2 incubator with the cells in the cell seeding channel focused under a X10 objective, and a 24-h observation interval was set to capture images every 5 min. Following a period of 24 h, the recordings were analyzed using the M4 Studio tracking software version 2.6.2. (Phase Holographic Imaging AB).

Western blot analysis. For protein expression analyses, GC1415 cells ($1x10^6$ cells) alone or with auto-TMVs (3 μg) were incubated for 0.5, 2 and 24 h (37˚C; 5% CO_2) in a CO_2 incubator. Cell lysates were then prepared and electrophoresis was performed, as previously described (21). A total of 20 μg lysed protein of each sample was heated (70˚C; 10 min) and electrophoresis was performed in 14% polyacrylamide gel. The proteins were then transferred onto PVDF membranes, blocked (room temperature; 1 h) using Tris-Buffered Saline with 0.1% Tween and 1% bovine serum albumin (TTBS) and incubated (overnight; 4˚C) with the following monoclonal antibodies (mAbs; all, 1:1,000): Rabbit anti-phospho-AKT (cat. no. 4060S), anti-phospho-p44/42 MAP kinase (cat. no. 9106S) and anti-GAPDH (cat. no. 2118; all, Cell Signaling Technology, Inc.). The membranes were subsequently washed in TTBS and incubated with secondary goat anti-rabbit antibody (cat. no. 7074S; Cell Signaling Technology, Inc.; 1:4,000) conjugated with horseradish peroxidase (HRP) at room temperature for 1 h. The protein bands were visualized using SuperSignal West Pico PLUS Chemiluminescent Substrate (Thermo Fisher Scientific, Inc.) and analyzed with the Kodak Gel Logic 1500 imaging system (Kodak). Where applicable, densitometric analysis was performed using the Kodak Molecular Imaging software version 4.5.0 (Kodak). Additionally, lysates obtained from auto-TMVs alone (20 μg) were tested for the presence of exosomal markers, including Alix, CD9 and CD63, using the same protocol as aforementioned. The following mAbs (all, 1:1,000) were used: Mouse anti-Alix (cat. no. 2171; Cell Signaling Technology, Inc.), rabbit anti-CD9 (cat. no. 13174; Cell Signaling Technology, Inc.) and rabbit anti-CD63 (cat. no. sc5275; Santa-Cruz Biotechnology, Inc.). The following secondary antibodies were used (all HRP-conjugated, 1:4,000): for Alix detection-horse anti-mouse (cat. no. 7076P2, Cell Signaling Technology, Inc.) and for CD9 and CD63 detection-goat anti-rabbit (cat. no. 7074S, Cell Signaling Technology, Inc.). Visualization of the respective proteins was performed as aforementioned.

Cellular respiration. For the assessment of mitochondrial respiration, the oxygen consumption rate (Ocr) was measured using the Seahorse XF analyzer and the Seahorse XF Cell Mito Stress Test, according to the manufacturer's protocol (Agilent Technologies, Inc.). The GC1415 cells ($2x10^4$) were suspended in the DMEM cell culture medium supplemented with 5% FBS and transferred into wells of Cell Culture Miniplates (Agilent Technologies, Inc.) to allow overnight cell seeding under standard conditions (37˚C; 5% CO_2). To achieve the required stability, the chambers of the Extracellular Flux Cartridge (Agilent Technologies, Inc.) were filled with the XF Calibrant (Agilent Technologies, Inc.) and placed overnight in an incubator (37˚C) without CO_2. After a period of 24 h, the culture medium was carefully aspirated and discarded, and the GC1415 cells were washed twice with 200 μl pre-warmed (37˚C) stabilized Seahorse Medium (Agilent Technologies, Inc.) that was prepared according to the manufacturer's protocol. A total of 180 μl Seahorse Medium was added to each well containing the washed GC1415 cells, and the Cell Culture Miniplate was then placed in an incubator (37˚C) without CO_2 for 1 h. Using the Seahorse Medium, concentrations of auto-TMVs (3 μg), oligomycin, *p*-triflouro-methoxyphenylhydrazone and rotenone/antimycin A (all from Agilent Technologies, Inc.) mix were prepared and loaded into the appropriate chambers of the calibrated Extracellular Flux Cartridge, which was then placed into the Seahorse XF analyzer. The stabilized Cell Culture Miniplate containing the GC1415 tumor cells was then placed into the Seahorse XF analyzer and the Acute Injection Seahorse XF Cell Mito Stress Test protocol was started with the initial injection of auto-TMVs. The GC1415 cells from each of the wells were subsequently lysed using the M-PER reagent (Thermo Fisher Scientific, Inc.) and their protein concentration was assessed (Bradford assay) for normalization. All the results were analyzed using Wave software version 2.6.0.31 (Agilent Technologies, Inc.).

Statistical analysis. All the data in the present study were analyzed using GraphPad software version 5.0 (GraphPad Software, Inc.) and are presented as the means ± standard error of the mean. An unpaired Student's t-test (western blot densitometric analysis) and one-way ANOVA followed by Dunnett's post hoc test (Ocr analysis) were used to assess the differences among groups. $P<0.05$ was considered to indicate a statistically significant difference.

Results

Characterization of auto-TMVs. The NTA indicated the size range of auto-TMVs to be 90-800 nm, demonstrating that the predominant population of studied vesicles was composed of microvesicles (Fig. 1A), which, according to the position statement of the International Society for Extracellular Vesicles on minimal information for studies of extracellular vesicles 2018 guidelines, are defined as medium/large EVs (22). The average size of the analyzed auto-TMVs was 160.7 nm, and their modal size was 124 nm. An image of auto-TMVs obtained using SEM confirmed these results (Fig. 1B). Western blot analysis revealed the presence of endosomal/cytosolic markers (Alix and CD9; Fig. 1C) in auto-TMVs, indicating that they are composed, in part, of a population that exhibits an intracellular origin.

PCR arrays. The gene expression data identified the overexpression of 75 genes and the underexpression of 96 genes in GC1415 cells following interaction with auto-TMVs. These genes included oncogenes, tumor suppressor genes and genes

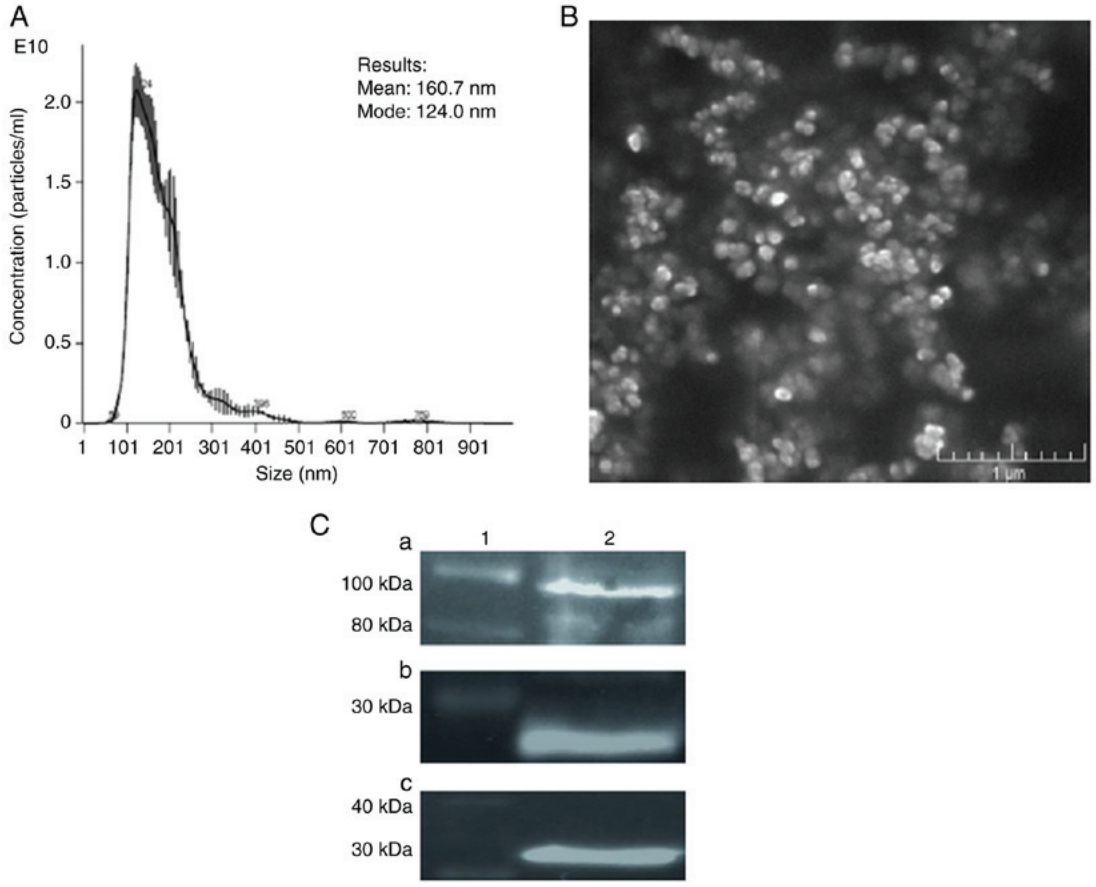

Figure 1. Characterization of auto-TMVs. (A) Size range of auto-TMVs obtained using nanoparticle tracking analysis. Data are from one representative experiment (n=3). (B) An image of auto-TMVs obtained using scanning electron microscopy. (C) Protein expression of (a) Alix, (b) CD9 and (c) GAPDH in auto-TMVs. Lane 1, size marker; lane 2, auto-TMVs; auto-TMVs, autologous tumor-derived microvesicles.

associated with angiogenesis and metastasis. A number of the overexpressed genes included genes that code for transcription factors or their co-activators [including *MYC,* forkhead box D3 (*FOXD3*), *MYB,* ETS Proto-Oncogene 1 (*ETS1*), ETS Transcription Factor *ELK1* (*ELK1*), *JUNB,* transcription factor protein 20 *(TCF20)* and *FOS*; Fig. 2A], with *TCF20* exhibiting the highest fold increase (16.85). Another set of overexpressed genes included genes that code for proteins with kinase activity [including phosphatidylinositol-4-phosphate 3-kinase catalytic subunit type 2 alpha (*PIK3C2A*), Janus kinase 2 (*JAK-2*), fibroblast growth factor receptor 4 (*FGFR4*), *AKT-1* and *CDK4*; Fig. 2B], receptor tyrosine kinases (RTKs), including [Fms related tyrosine kinase 1 (*FLT1*), *RET, MET, KIT* and Erb-B2 receptor tyrosine kinase 2 (*ERBB2*); Fig. 2C] and their potential ligands [including KIT ligand (*KITLG*) and epidermal growth factor (*EGF*); Fig. 2C]. In the protein kinase group, the *AKT-1* gene exhibited the highest fold increase (3.31), *ERBB2* indicated the highest fold increase in the RTK group (4.29) and *EGF* exhibited the highest fold increase in the RTKs ligands group (2.5) compared to the control. A large number of affected transcripts comprised of tissue inhibitors of metalloproteinases (TIMPs; including *TIMP-1, -2, -3* and *-4*; Fig. 2D) and matrix metalloproteinases (MMPs; including *MMP-2, -9, -11* and *-14*; Fig. 2D). In the current study, all the transcripts were downregulated apart from *TIMP-2,* which was slightly elevated with a fold increase at 1.10. The mRNA expression of chemokine ligands presented a more challenging scenario. In this case, a number of genes were underexpressed [including C-C motif chemokine ligand (*CCL)2, CCL7,* C-X-C motif chemokine ligand (*CXCL)1* and *CXCL5*; Fig. 2E], while other genes were overexpressed (including *CXCL6, CXCL9 and CXCL12*; Fig. 3E). The obtained data also indicated an association between the tumor suppressor protein p53 (*TP53*), which was downregulated (6.79) and mouse double minute 2 homolog (*MDM2*), which was upregulated (3.35; Fig. 2F). Other mRNA transcripts that were substantially overexpressed in the GC1415 cells following contact with auto-TMV, including methionine aminopeptidase 2 [(*METAP2*); 7.33-fold increase], interleukin-1 β [(*IL1-β*); 7.95-fold increase] and nitric oxide synthase 3 [(*NOS3*); 6.88-fold increase; Fig. S1]. The expression heatmaps of all tested genes are presented in Fig. S1.

Chemotaxis. The average migration distance by the control GC1415 cells was 71.6 μm over a period of 12 h. The average motility speed over a period of 12 h was 31.15 μm/h with the highest speed being recorded at 11 h (46.7 μm/h). The average distance migrated by the GC1415 cells towards their auto-TMVs gradient was 80.5 μm over a period of 12 h. The average motility speed for the same time period was 27.20 μm/h with the highest being 59.3 μm/h, which was observed at the 10 min mark of the experiment. However, the average motility speed was lower for the GC1415 cells exposed to the auto-TMVs gradient, and they covered a higher distance

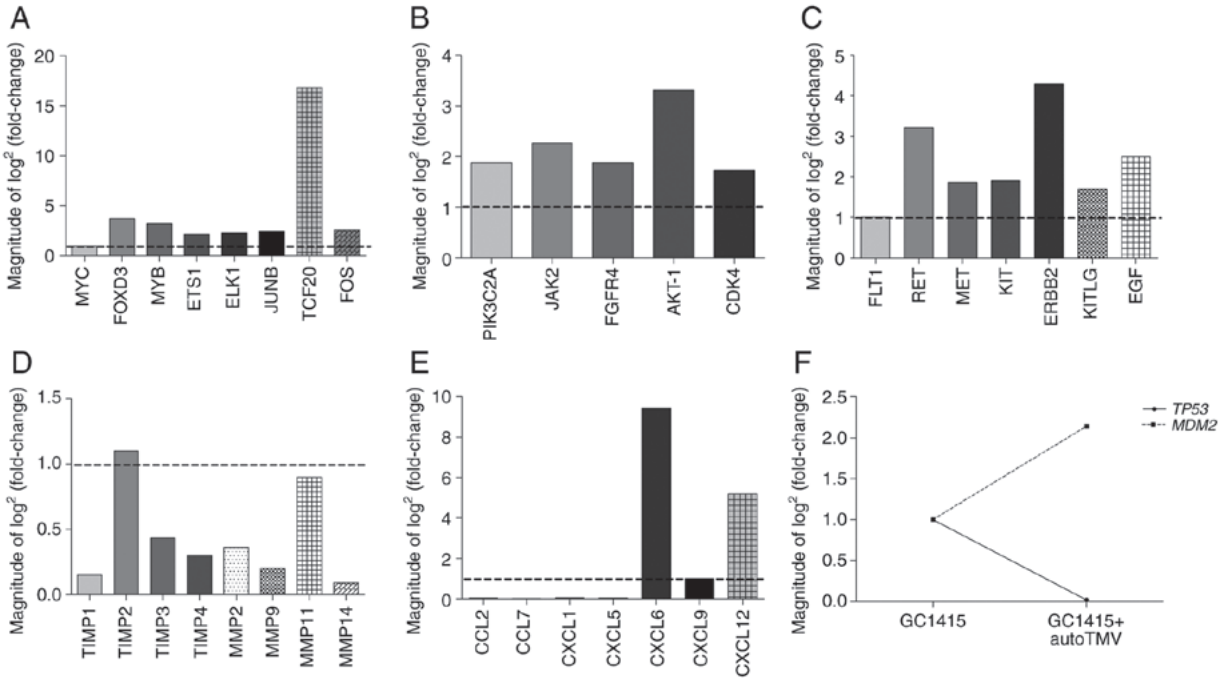

Figure 2. Effect of auto-TMVs on mRNA gene expression in GC1415 cells. Fold change in mRNA gene expression of (A) transcription factors, (B) protein kinases, (C) receptor tyrosine kinases and their ligands, (D) tissue inhibitors of metalloproteinases and matrix metalloproteinases, (E) chemokines and (F) tumor suppressor protein 53 and mouse double minute 2 homolog. Dashed line signifies the controls (n=2). Auto-TMVs, autologous tumor-derived microvesicles.

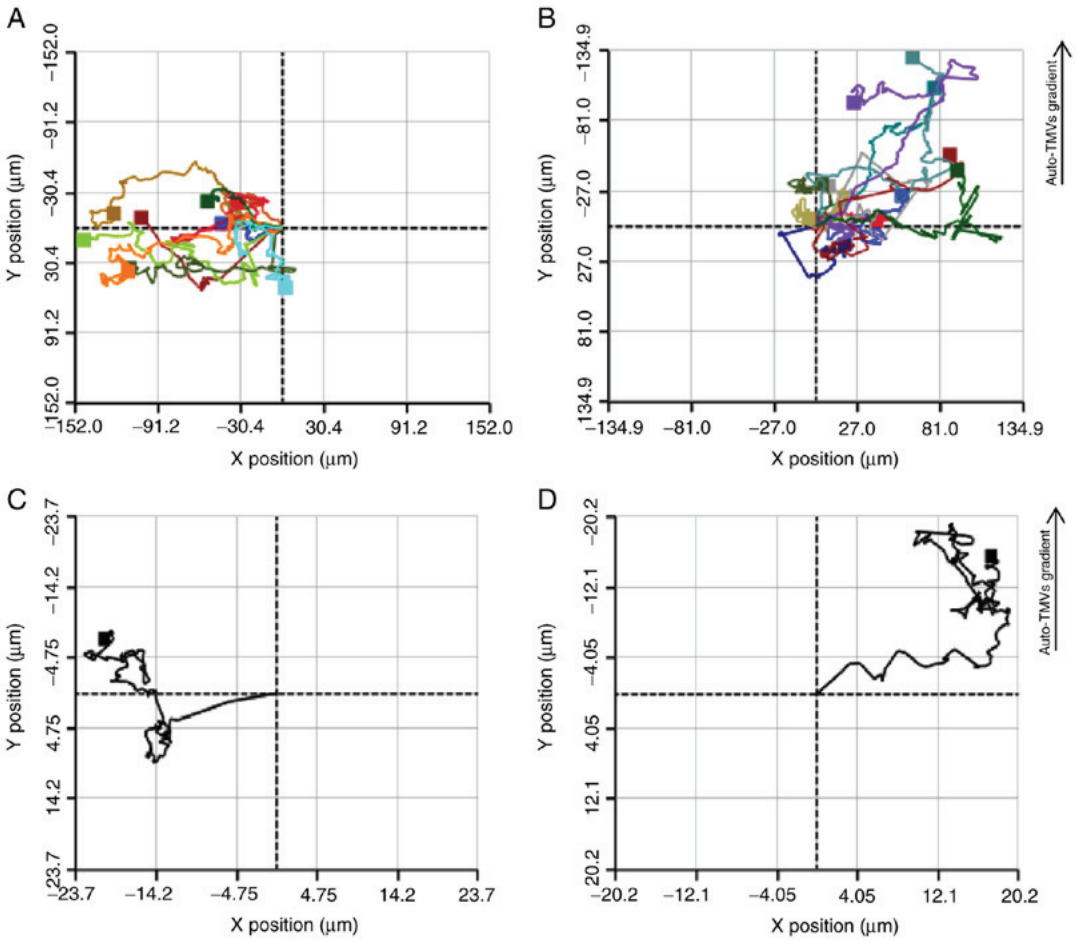

Figure 3. Upper panels depict the raw migration pattern of (A) GC1415 cells alone and (B) GC1415 cells exposed to auto-TMV gradient. The lower panels depict the average migration pattern of (C) GC1415 cells alone and (D) GC1415 cells exposed to auto-TMVs gradient. Each colored line represents a single cell migration pattern. Data are from one representative experiment (n=3). Auto-TMVs, autologous tumor-derived microvesicles.

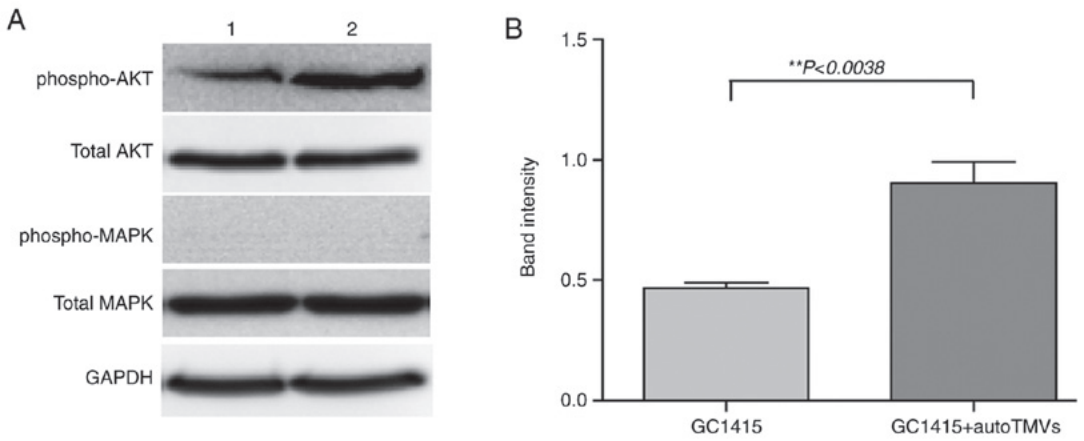

Figure 4. Western blot analysis of (A) phospho-AKT and phospho-MAPK protein expression in (lane 1) GC1415 cells alone and (lane 2) GC1415 cells treated with auto-TMVs. (B) Densitometric analysis of phospho-AKT bands normalized to total AKT bands (n=4). Auto-TMVs, autologous tumor-derived microvesicles.

compared with control GC1415 cells. Additionally, the migration tracking graph of GC1415 cells exposed to the auto-TMVs gradient, as presented in Fig. 3, exhibited a more orderly pattern compared with the control GC1415 cells, implying the chemoattractant capabilities of auto-TMVs. The highest motility speed for the gradient-exposed GC1415 cells was observed almost immediately (10 min) after the cell tracking was initiated when compared with the control GC1415 cells, which was recorded at the 11-h time point.

Western blot analysis. The PI3K/AKT and MAPK/ERK signaling pathways were analyzed in the GC1415 cells and in the GC1415 cells treated with auto-TMVs at time intervals of 0.5, 2 and 24 h. The MAPK/ERK signaling pathway constituents (p44/p42 MAP kinase) were not indicated to be influenced by auto-TMVs at any of the tested time points (Fig. 4A). However, an increase in the phosphorylated form of AKT kinase (phospho-AKT; Fig. 4A and B) was observed at the 0.5 h time point, indicating that auto-TMVs-stimulated signal transduction may occur via the PI3K/AKT pathway.

Cellular respiration. Treatment of the GC1415 cells with auto-TMVs resulted in a decrease in the Ocr compared with the control GC1415 cells, as presented in Fig. 5, indicating a decrease in mitochondrial respiration. The Ocr values measured during the basal respiration phase were decreased in treated GC1415 cells, which suggested that auto-TMVs decreased initial cellular energy requirements (Fig. 6A). This decrease in cellular energy demand was also evident during the ATP production phase of the experiment and in the Ocr values obtained for the spare respiratory capacity measurements (Fig. 6B and C).

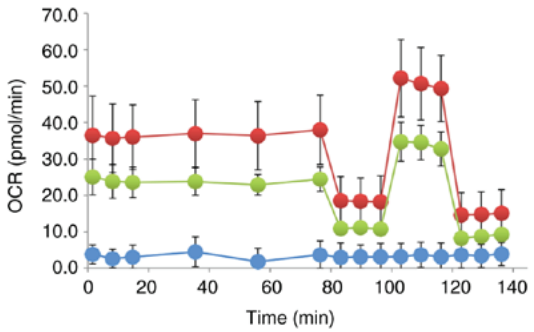

Figure 5. The Cell Mito Stress Test profile presenting Ocr values for auto-TMVs (blue), GC1415 cells alone (red) and GC1415 cells treated with auto-TMVs (green). All measurements were performed in duplicate. Data are from one representative experiment (n=4). Ocr, oxygen consumption rate; auto-TMVs, Autologous tumor-derived microvesicles.

Discussion

Cancer develops as a consequence of the continual and uncontrolled proliferation of cells, the outcome of which is an unfavorable transformation, leading to the invasion of normal tissue/organs and throughout the body (23). The loss of responsiveness of cancer cells to signals controlling normal cell behavior is a result of abnormalities that develop in multiple cell regulatory systems. The current study demonstrated that a number of genes, protein expression and cell behavior/metabolism are affected in auto-TMV-exposed GC1415 cells and this may suggest that, auto-TMVs play a role in facilitating cancer proliferation and metastasis.

An abnormal gene expression profile in cancer cells is associated with their potential to proliferate and spread (23). The data obtained in the current study indicated a variety of genes that were affected in GC1415 cells following contact with auto-TMVs. For example, TCF20 mRNA, which was highly overexpressed (Fig. 2A), is a transcriptional coactivator that enhances the activity of Jun and Sp1 transcription factors (24). With the Fos subunit, Jun can form AP-1 transcription factor, which can bind to the promoter gene regions of a number of genes (including *IL-2, CD95L, MMP-1* and *TGF-β*) that are associated with cell proliferation, differentiation and apoptosis (22-25). Sp1 is also a transcription factor that binds GC/GT-rich promoter elements through its zinc fingers and has been indicated to play a role in tumor growth and metastasis by regulating cell cycle genes and VEGF (24). Genes encoding TIMPs, which are glycoproteins that are natural inhibitors of MMPs-peptides and are associated with the degradation of the extracellular matrix (26,27), were also

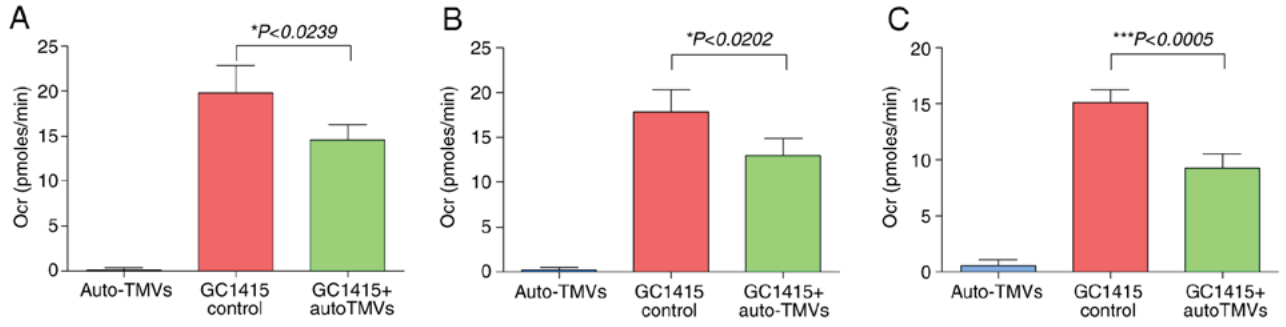

Figure 6. Ocr values obtained during (A) basal respiration, (B) ATP production and (C) spare respiratory capacity measurements in auto-TMVs alone (blue), control GC1415 cells (red) and GC1415 cells treated with auto-TMVs (green; n=4); *P<0.05 and ***P<0.0005. Ocr, oxygen consumption rate; auto-TMVs, autologous tumor-derived microvesicles.

affected (underexpressed) in auto-TMVs-exposed GC1415 cells (Fig. 2D). This indicated their potential involvement in metastasis. A simultaneous underexpression of MMP (including, *MMP-2, -9, -11 and -14*; Fig. 2D) mRNA transcripts was also observed. However, the downregulation of TIMP mRNA transcripts was demonstrated, MMP mRNA underexpression and its significance requires future investigation. The results of the current study indicated an association between *TP53* and *MDM2* transcript expression (Fig. 2F), which may also imply that auto-TMVs may be initiating mechanisms in GC1415 cells that increase tumor proliferation. The p53 protein is a known tumor suppressor that is capable of initiating DNA damage repair, apoptosis and/or cell cycle arrest in affected cells, which are important mechanisms in tumorigenesis (28,29). The MDM2 protein, selectively binds to the p53 protein, and causes its inactivation, which limits its anticancer potential (30,31).

The interaction between antigens and surface receptors initiates an intracellular signaling cascade that generates an appropriate cellular response (23). However, the mechanisms through which auto-TMVs initiate the PI3K/AKT signaling pathway in GC1415 cells has not yet been determined. However, this may be associated with one of the receptors exhibiting tyrosine kinase activity (namely RTKs) (30-32). The expression of HER-2/neu receptor, a member of the RTK family, on GC1415 cells, has been previously reported (18). In the current study, the upregulation of *HER/2 neu* (*ERBB2*) mRNA gene expression (Fig. 2C) was observed in GC1415 cells treated with auto-TMVs, and this result may demonstrate its involvement in signal transduction. The overexpression of *HER/2 neu* (*ERBB2*) protein and its mRNA has been reported in a variety of tumor types, which may lead to the activation of downstream protein kinases and transcription factors that can propagate tumor progression and metastasis (29-33). The simultaneous upregulation of *AKT-1* mRNA (Fig. 2A) and the phosphorylated form of AKT 1 kinase protein (Fig. 4A), in auto-TMV-exposed GC1415 cells, support this hypothesis. Additionally, it has been reported that AKT-1, through the activation of mTOR, induces hypoxia-inducible factor 1α levels, which is a complex that is responsible for binding to hypoxia-responsible elements of the promoters of genes coding for glycolytic enzymes (34). This is in concurrence with the results of the current study, which indicated a decrease in the Ocrs (Figs. 5 and 6), suggesting that contact with auto-TMVs may cause a metabolic switch from oxidative phosphorylation to glycolysis in GC1415 cells, a phenomenon frequently observed in tumor metabolism and referred to as the Warburg effect (35). It should be pointed out, however, that the observed Ocrs were relatively low (~40 pmol/min), which, in part, may be explained by the low auto-TMVs concentration (3 μg) used in the experiments. During growth, tumor cells require increasing amounts of energy to meet their cellular demands (34,36,37). Glycolysis, although not as efficient as oxidative phosphorylation, metabolizes glucose more rapidly and delivers ATP to growing tumors at a faster rate (38). Additionally, intermediates generated during glycolysis have been indicated to be shunted into subsidiary pathways causing the *de novo* generation of nucleotides, lipids and amino acids, which can be utilized by tumor cells to propagate further proliferation (39).

Metastasis is the final stage of cancer and requires a migratory ability of cancer cells that is facilitated by surface chemokine receptors that are present at the cell surface (35,38,39). A higher expression of CXCR4, CXCR7 and their ligand, CXCL12/SDF-1, has been observed in GC cells, particularly in the intestinal-type, where it has been associated with lymph node and liver metastasis (40,41). Previous phenotyping has revealed that GC1415 cells express a number of chemokine receptors, including CXCR4 (17). However, in this aforementioned study, CXCR4 expression was relatively low (<10%) (17). Other researchers have revealed that exposure of the GC1415 cells to auto-TMVs induces an enhancement of tumor growth and cancer-cell induced angiogenesis in NOD-SCID mice (18). It has also been previously reported that surface receptors and mRNA transcripts can be transferred to target cells by EVs (40-42). The gene expression data acquired in the current study demonstrated that CXCR4 and its ligand's (CXCL12/SDF-1) mRNA were upregulated in GC1415 cells treated with auto-TMVs and this may indicate their chemotactic abilities (Figs. 2E and S1A). The CXCR4 receptor and its mRNA may be transferred to GC1415 cells via auto-TMVs, which may lead to an instant enhancement in the receptor's surface expression, or *de novo* synthesis from the transferred mRNA transcript. However, the CXCL12 mRNA translation in exposed GC1415 cells may lead to the synthesis of the ligand and its potential release *via* auto-TMVs, which may serve as a chemoattractant for CXCR4^{+} cells.

The aim of the present study was to assess the effects of auto-TMVs on GC1415 cells. The initial characterization of auto-TMVs revealed their size range as 90-800 nm with an average size of 160.7 nm, suggesting that the majority of auto-TMVs are within the same size range as microvesicles. The obtained gene expression data indicated an array of genes to be overexpressed and underexpressed in GC1415 cells that were exposed to auto-TMVs. These genes coding for proteins engaged in cellular processes, including signal transduction, metabolism, chemotaxis, angiogenesis and metastasis. Chemotaxis experiments performed in the present study revealed that GC1415 cells migrated towards their auto-TMVs gradient. Signal transduction experiments performed in the current study indicated the PI3K/AKT signaling pathway to be affected in auto-TMVs-exposed GC1415 cells. The obtained data on cellular metabolism in GC1415 cells exposed to auto-TMVs have revealed a metabolic shift from oxidative phosphorylation to glycolysis.

In conclusion, the data from the current study demonstrate that EVs released by tumor cells may also interact and induce behavioral changes under *in vitro* conditions in other tumor cells. These changes may enhance pro-tumorigenic activity in cancer cells interacting with auto-TMVs. Further studies focusing on the individual aspects of the presented data (including signal transduction, metabolism and chemotaxis) will provide increased knowledge regarding the effect of autologous TMVs on tumor cells.

Acknowledgements

The authors would like to thank Professor Joanna Cichy and Dr Mateusz Kwitniewski (both, Department of Immunology, Jagiellonian University) for disclosing the Seahorse XF Analyzer and providing assistance with the cellular respiration experiments.

Funding

This research was funded by National Science Centre, grant no. 2012/07/B/NZ6/03499 and European Commission H2020-MSCA-RISE-2017; grant no. 777682 'CANCER'.

Availability of data and materials

All data generated or analyzed during this study are included in this published article or are available from the corresponding author on reasonable request.

Authors' contributions

RS and MBK were involved in the conception and design of the study. RS, KW, MBK, MSt, JB and MSi were involved in the study methodology. MPW was involved in SEM imaging. RS, KW and MBK were involved in data acquisition. RS was involved in data analysis. RS was involved in the writing and preparation of the original draft. RS, MBK, JB and MSi were involved in the writing, reviewing and editing of the article. RS and MBK were involved in study supervision. RS was also involved in project administration. All authors have read and approved the final manuscript.

Ethics approval and consent to participate

Not applicable.

Patient consent for publication

Not applicable.

Competing interests

The authors declare that they have no competing interests.

References

1. Yada T, Yokoi C and Uemura N: The current state of diagnosis and treatment for early gastric cancer. Diagn Ther Endosc 2013: 241320, 2013.
2. Ferlay J, Shin HR, Bray F, Forman D, Mathers C and Parkin DM: Estimates of worldwide burden of cancer in 2008: GLOBOCAN 2008. Int J Cancer 127: 2893-2917, 2010.
3. Jemal A, Bray F, Center MM, Ferlay J, Ward E and Forman D: Global cancer statistics. CA Cancer J Clin 61: 69-90, 2011.
4. Parkin DM, Bray FI and Devesa SS: Cancer burden in the year 2000. The global picture. Eur J Cancer 37 (Suppl 8): S4-S66, 2001.
5. Parkin DM: International variation. Oncogene 23: 6329-6340, 2004.
6. Ratajczak J, Wysoczynski M, Hayek F, Janowska-Wieczorek A and Ratajczak MZ: Membrane-derived microvesicles: Important and underappreciated mediators of cell-to-cell communication. Leukemia 20: 1487-1495, 2006.
7. van der Pol E, Hoekstra AG, Sturk A, Otto C, van Leeuwen TG and Nieuwland R: Optical and non-optical methods for detection and characterization of microparticles and exosomes. J Thromb Haemost 8: 2596-2607, 2010.
8. Cocucci E, Racchetti G and Meldolesi J: Shedding microvesicles: Artefacts no more. Trends Cell Biol 19: 43-51, 2009.
9. Baj-Krzyworzeka M, Szatanek R, Weglarczyk K, Baran J, Urbanowicz B, Brański P, Ratajczak MZ and Zembala M: Tumour-derived microvesicles carry several surface determinants and mRNA of tumour cells and transfer some of these determinants to monocytes. Cancer Immunol Immunother 55: 808-818, 2006.
10. Valadi H, Ekström K, Bossios A, Sjöstrand M, Lee JJ and Lötvall JO: Exosome-mediated transfer of mRNAs and microRNAs is a novel mechanism of genetic exchange between cells. Nat Cell Biol 9: 654-659, 2007.
11. Webber J, Steadman R, Mason MD, Tabi Z and Clayton A: Cancer exosomes trigger fibroblast to myofibroblast differentiation. Cancer Res 70: 9621-9630, 2010.
12. Sidhu SS, Mengistab AT, Tauscher AN, LaVail J and Basbaum C: The microvesicle as a vehicle for EMMPRin in tumor-stromal interactions. Oncogene 23: 956-963, 2004.
13. Wieckowski EU, Visus C, Szajnik M, Szczepanski MJ, Storkus WJ and Whiteside TL: Tumor-derived microvesicles promote regulatory T cell expansion and induce apoptosis in tumor-reactive activated CD8+ T lymphocytes. J Immunol 183: 3720-3730, 2009.
14. Gamperl H, Plattfaut C, Freund A, Quecke T, Theophil F and Gieseler F: Extracellular vesicles from malignant effusions induce tumor cell migration: Inhibitory effect of LMWH tinzaparin. Cell Biol Int 40: 1050-1061, 2016.
15. Ristorcelli E, Beraud E, Mathieu S, Lombardo D and Verine A: Essential role of Notch signaling in apoptosis of human pancreatic tumoral cells mediated by exosomal nanoparticles. Int J Cancer 125: 1016-1026, 2009.
16. Al-Nedawi K, Meehan B, Micallef J, Lhotak V, May L, Guha A and Rak J: Intercellular transfer of the oncogenic receptor EGFRvIII by microvesicles derived from tumour cells. Nat Cell Biol 10: 619-624, 2008.
17. Mytar B, Stec M, Szatanek R, Węglarczyk K, Szewczyk K, Szczepanik A, Drabik G, Baran J, Siedlar M and Baj-Krzyworzeka M: Characterization of human gastric adenocarcinoma cell lines established from peritoneal ascites. Oncol Lett 15: 4849-4858, 2018.

18. Stec M, Szatanek R, Baj-Krzyworzeka M, Baran J, Zembala M, Barbasz J, Waligórska A, Dobrucki JW, Mytar B, Szczepanik A, *et al*: Interactions of tumour-derived micro(nano) vesicles with human gastric cancer cells. J Transl Med 13: 376, 2015.
19. Baj-Krzyworzeka M, Mytar B, Szatanek R, Surmiak M, Węglarczyk K, Baran J and Siedlar M: Colorectal cancer-derived microvesicles modulate differentiation of human monocytes to macrophages. J Transl Med 14: 36, 2016.
20. Szatanek R, Drabik G, Baran J, Kolodziejczyk P, Kulig J, Stachura J and Zembala M: Detection of isolated tumour cells in the blood and bone marrow of patients with gastric cancer by combined sorting, isolation and determination of MAGE-1, -2 mRNA expression. Oncol Rep 19: 1055-1060, 2008.
21. Rutkowska-Zapała M, Suski M, Szatanek R, Lenart M, Węglarczyk K, Olszanecki R, Grodzicki T, Strach M, Gąsowski J and Siedlar M: Human monocyte subsets exhibit divergent angiotensin I-converting activity. Clin Exp Immunol 181: 126-132, 2015.
22. Théry C, Witwer KW, Aikawa E, Alcaraz MJ, Anderson JD, Andriantsitohaina R, Antoniou A, Arab T, Archer F, Atkin-Smith GK, *et al*: Minimal information for studies of extracellular vesicles 2018 (MISEV2018): A position statement of the international society for extracellular vesicles and update of the MISEV2014 guidelines. J Extracell Vesicles 7: 1535750, 2018.
23. Feitelson MA, Arzumanyan A, Kulathinal RJ, Blain SW, Holcombe RF, Mahajna J, Marino M, Martinez-Chantar ML, Nawroth R, Sanchez-Garcia I, *et al*: Sustained proliferation in cancer: Mechanisms and novel therapeutic targets. Semin Cancer Biol 35 (Suppl): S25-S54, 2015.
24. Safe S and Abdelrahim M: Sp transcription factor family and its role in cancer. Eur J Cancer 41: 2438-2448, 2005.
25. McMurray RW, Ndebele K, Hardy KJ and Jenkins JK: 17-beta-estradiol suppresses IL-2 and IL-2 receptor. Cytokine 14: 324-333, 2001.
26. Gialeli C, Theocharis AD and Karamanos NK: Roles of matrix metalloproteinases in cancer progression and their pharmacological targeting. FEBS J 278: 16-27, 2011.
27. Kessenbrock K, Plaks V and Werb Z: Matrix metalloproteinases: Regulators of the tumor microenvironment. Cell 141: 52-67, 2010.
28. Sionov RV and Haupt Y: The cellular response to p53: The decision between life and death. Oncogene 18: 6145-6157, 1999.
29. Prives C and Hall PA: The p53 pathway. J Pathol 187: 112-26, 1999.
30. Kubbutat MH, Jones SN and Vousden KH: Regulation of p53 stability by Mdm2. Nature 387: 299-303, 1997.
31. Haupt Y, Maya R, Kazaz A and Oren M: Mdm2 promotes the rapid degradation of p53. Nature 387: 296-299, 1997.
32. Iyer P, Shrikhande SV, Ranjan M, Joshi A, Gardi N, Prasad R, Dharavath B, Thorat R, Salunkhe S, Sahoo B, *et al*: ERBB2 and KRAS alterations mediate response to EGFR inhibitors in early stage gallbladder cancer. Int J Cancer 144: 2008-2019, 2018.
33. Slamon DJ, Godolphin W, Jones LA, Holt JA, Wong SG, Keith DE, Levin WJ, Stuart SG, Udove J, Ullrich A, *et al*: Studies of the HER-2/neu proto-oncogene in human breast and ovarian cancer. Science 244: 707-712, 1989.
34. Shaw RJ: Glucose metabolism and cancer. Curr Opin Cell Biol 18: 598-608, 2006.
35. WARBURG O: Origin of cancer cells. Oncologia 9: 75-83, 1956 (In German).
36. Azarhoosh R, Ebneghasem R and Besharat S: HER-2/neu gene amplification in gastric adenocarcinoma and its relationship with clinical and pathological findings. J Gastrointest Oncol 8: 1046-1050, 2017.
37. Tateishi M, Ishida T, Mitsudomi T, Kaneko S and Sugimachi K: Prognostic value of c-erbB-2 protein expression in human lung adenocarcinoma and squamous cell carcinoma. Eur J Cancer 27: 1372-1375, 1991.
38. Pfeiffer T, Schuster S and Bonhoeffer S: Cooperation and competition in the evolution of ATP-producing pathways. Science 292: 504-507, 2001.
39. Hamanaka RB and Chandel NS: Targeting glucose metabolism for cancer therapy. J Exp Med 209: 211-215, 2012.
40. Iwasa S, Yanagawa T, Fan J and Katoh R: Expression of CXCR4 and its ligand SDF-1 in intestinal-type gastric cancer is associated with lymph node and liver metastasis. Anticancer Res 29: 4751-4758, 2009.
41. Ma DM, Luo DX and Zhang J: SDF-1/CXCR7 axis regulates the proliferation, invasion, adhesion, and angiogenesis of gastric cancer cells. World J Surg Oncol 14: 256, 2016.
42. Okuma A, Hanyu A, Watanabe S and Hara E: $p16^{Ink4a}$ and $p21^{Cip1/Waf1}$ promote tumour growth by enhancing myeloid-derived suppressor cells chemotaxis. Nat Commun 8: 2050, 2017.